Suzaku Observation of Two Ultraluminous X-Ray Sources in NGC 1313

T. Mizuno, [1] R. Miyawaki, [2] K. Ebisawa,[3] A. Kubota, [4] M. Miyamoto, [5] L. Winter, [6] Y. Ueda,[7] N. Isobe,[4] G. Dewangan,[8] C. Done,[9] R. E. Griffiths,[8] Y. Haba,[10] M. Kokubun,[2] J. Kotoku,[11] K. Makishima,[2,4] K. Matsushita,[5] R. F. Mushotzky,[6] M. Namiki,[12] R. Petre,[6] H. Takahashi,[1] T. Tamagawa,[4] and Y. Terashima *,[3]

[1] *Department of Physics, Hiroshima University, 1-3-1 Kagamiyama, Higashi-Hiroshima, Hiroshima 739-852*
mizuno@hepl.hiroshima-u.ac.jp

[2] *Department of Physics, University of Tokyo, 7-3-1 Hongo, Bunkyo-ku, Tokyo 113-0033*

[3] *Institute of Space and Astronautical Science, Japan Aerospace Exploration Agency, 3-1-1 Yoshinodai, Sagamihara, Kanagawa 229-8510*

[4] *Institute of Physical and Chemical Research (RIKEN), 2-1 Hirosawa, Wako, Saitama 351-0198*

[5] *Department of Physics, Tokyo University of Science, 1-3 Kagurazaka, Shinjuku-ku, Tokyo 162-8601*

[6] *Exploration of the Universe Division, NASA Goddard Space Flight Center, Greenbelt, MD 20771, USA*

[7] *Department of Physics, Kyoto University, Sakyo-ku, Kyoto 606-8502*

[8] *Department of Physics, Carnegie Mellon University, 5000 Forbes Avenue, Pittsburgh, PA 15213, USA*

[9] *Department of Physics, University of Durham, South Road, Durham, DH1 3LE, UK*

[10] *Department of Physics, Nagoya University, Furo-cho, Chikusa, Nagoya 464-8602*

[11] *Department of Physics, Tokyo Institute of Technology, 2-12-1, Meguro-ku, Ohokayama, Tokyo 152-8551*

[12] *Department of Earth and Space Science, Osaka University, 1-1 Machikaneyama-cho, Toyonaka, Osaka 560-0*

(Received 2000 December 31; accepted 2001 January 1)

Abstract

A study was made of two ultraluminous X-ray sources (ULXs) in the nearby face-on, late-type Sb galaxy NGC 1313 using data from Suzaku, the 5th Japanese X-ray satellite. Within the 90 ks observation, both sources named X-1 and X-2 exhibited luminosity change by about 50 %. The 0.4–10 keV X-ray luminosity was measured to be 2.5×10^{40} erg s^{-1} and 5.8×10^{39} erg s^{-1} for X-1 and X-2, respectively, requiring a black hole of 50–200$M_{\odot}$ in order not to exceed the Eddington limit. For X-1, the spectrum exhibited a strong power-law component with a high energy cutoff which is thought to arise from strong Comptonization by a disk corona, suggesting the source was in a very high state. Absorption line features with equivalent widths of 40–80 eV found at 7.0 keV and 7.8 keV in the X-1 spectrum support the presence of a highly ionized plasma and a high mass accretion rate on the system. Oxygen abundance of the NGC 1313 circumstellar matter toward X-1 was found to be subsolar, viz. O/H $= (5.0 \pm 1.0) \times 10^{-4}$. The spectrum of X-2 in fainter phase is best represented

by a multicolor disk blackbody model with $T_{\rm in} = 1.2$–1.3 keV and becomes flatter as the flux increases; the source is interpreted to be in a slim disk state.

Key words: accretion, accretion disks – black hole physics – X-rays: individual (NGC 1313 X-1; NGC 1313 X-2)

1. Introduction

Ultraluminous X-ray sources, or ULXs, are pointlike X-ray sources with bolometric luminosities in excess of 3×10^{39} erg s^{-1}. They were first discovered using the Einstein Observatory (for a review of the first decade of ULX discoveries, see Fabbbiano 1989), and have often been hypothesized to be massive accreting black-hole binaries (BHBs) because of their high luminosity and time variability. Assuming a simple geometry, an accreting mass of 30–100 $M_\odot$ is required so that the observed luminosities do not exceed the Eddingtion limit, although the firm evidence for this interpretation had been lacking for almost 20 years.

A breakthrough in the study of ULXs was brought about by observations with the ASCA satellite: more than a dozen ULXs were studied spectroscopically in the 0.5–10 keV energy range for the first time (e.g., Okada et al. 1998; Colbert, Mushotzky 1999; Makishima et al. 2000; Mizuno 2000). Spectra of the majority of the ASCA sample have been well modeled by a so-called multi-color disk model (MCD model: Mitsuda et al. 1984). Spectral transitions between the MCD-type state and the power-law type state, often seen in Galactic BHBs, have also been found in some ULXs (La Parola et al. 2001; Kubota et al. 2001a). These spectral characteristics generally reinforce the black hole scenario with masses of 30–100 $M_\odot$ for ULXs, although the apparent properties of high disk temperatures (innermost disk temperature $T_{\rm in}$ within the range 1.0–1.8 keV; Makishima et al. 2000) and the change of innermost disk radius (Mizuno et al. 2001) both distinguish them from simple scaled-up versions of stellar-mass BHBs.

In the early 2000s, further advancements were provided from observations made with the Chandra and XMM-Newton Observatories. More than 150 off-nucleus sources, with liminosities exceeding 10^{39} erg s^{-1}, have been observed using Chandra, and all of them have been determined to be pointlike at 0.″5 angular resolution (Swartz et al. 2004). Some luminous ULXs were found to be associated with recent star formation activities, suggesting that they originate in young and short-lived systems. High-quality spectra of $\sim$ 30 ULXs, obtained using XMM, were in many cases dominated by a flat power-law like component, often accompanied by soft excess below 1 keV (e.g., Foschini et al. 2002; Feng, Kaaret 2005; Winter, Mushotzky, Reynolds 2005). This soft component could be interpreted as emission from a cool accretion disk (T_{in}=0.1–0.3 keV) around a massive black hole of $\sim 10^3$ $M_\odot$ (e.g., Miller et al. 2003; Miller et al. 2004), although this interpretation is still controversial (e.g., Dewangan et al. 2005; Stobbart et al.

* present address: Department of Physics, Ehime University, Bunkyo-cho, Matsuyama, Ehime 790-8577

2006; Goad et al. 2006).

Another important clue to the nature of ULXs has been provided through the study of Galactic BHBs. Besides the established two spectral states of BHBs, namely, the low/hard state with a dominant power-law continuum and the high/soft state dominated by an MCD emission (e.g., McClintock, Remillard 2003), two novel states have been identified mainly with RXTE observations of several BHBs (e.g., Kubota et al. 2001b; Kobayashi et al. 2003; Kubota, Makishima 2004). One is a so-called very high state, known since the 1990s (e.g., Miyamoto et al. 1991). As a source gets more luminous than in the soft state and enters this new state, its spectrum again becomes power-law like, presumably due to Comptonization by some hot plasmas, with the MCD component becoming weaker and sometimes cooler. By re-analyzing the ASCA data of IC 342 source 1, Kubota et al. (2002) showed that the observed power-law type spectrum of this ULX is suggestive of the very high state. The fourth state, characterized by an MCD-like but hotter spectra, is seen when a source is very luminous, close to or even exceeding the Eddington limit. As argued by Kubota, Makishima (2004) through the observation of Galactic BHB XTE J1550–564, this state may correspond to the theoretically predicted "slim disk" solution (e.g., Abramowicz et al. 1988; Szuszkiewicz et al. 1996; Watarai et al. 2000), in which an optically-thick disk with a moderate geometrical thickness is formed and advective cooling becomes important. The slim-disk interpretation successfully explains the high disk temperature and the changes of the disk radius observed from the most luminous class of ULXs (e.g., Mizuno et al. 2001; Ebisawa et al. 2003).

Another important characteristics of BHBs is the presence of absorption line features. With the improved spectral resolution realized by ASCA, Chandra and XMM-Newton, K absorption lines by highly ionized iron have been detected from neutron star binaries, active galactic nuclei and BHBs, allowing us to conduct detailed diagnostics of hot plasmas associated with those accreting systems (e.g., Ueda et al. 2004 and references therein). Detections of such absorption line features from ULXs would provide direct evidence of highly ionized ions around ULXs, and would further solidify their connection to Galactic BHBs. A possible absorption line at ~ 8 keV has been detected from Holmberg IX X-1 by Dewangan, Griffith, Rao (2006).

Despite the great progress described above, our understanding of ULXs is still far from satisfactory. In particular, it has been difficult to unambiguously distinguish different modelings of their spectra, and to understand how the spectrum changes as the source varies. In the present paper, we report our new Suzaku results on two ULXs (X-1 and X-2) in the nearby spiral galaxy NGC 1313. We suggest that X-1 was in a state which is very similar to the very high state of Galactic BHBs, while X-2 was in another state which may correspond to the slim disk solution. In addition, we have detected hints of Fe-K and Ni-K absorption lines in the X-1 spectra. Our new results also include possible indication of sub-solar Oxygen abundance in the X-ray absorption toward X-1.

2. Instrumentation and Observation

The 5th Japanese X-ray satellite Suzaku has several important instrumental properties which are suited to ULX studies. The X-ray Imaging Spectrometer (XIS; Koyama et al. 2006), combined with the X-ray Telescope (XRT; Serlemitsos et al. 2006), provides as our primary observing tool. Among the four XIS cameras, one (XIS1) utilizes a back-side illuminated CCD chip (BI chip), and realizes unprecedented sensitivity and energy resolution in the energy band below 1 keV. The other three XIS cameras, with front-side illuminated chips (FI chips), have an even better energy resolution, together with very low and stable background toward the hardest spectral end. As a result, the XIS plus XRT combination covers a very wide energy range, 0.2–12 keV, with a much flatter response than was achieved with previous missions. This in turn allows us to accurately constrain the continuum shape of ULXs, and to search for iron absorption/emission lines with a high sensitivity. In addition, the Hard X-ray Detector (HXD; Takahashi et al. 2006; Kokubun et al. 2006) realizes an unprecedented sensitivity in the energy range above 10 keV, and may detect the hard X-ray emission from the brightest ULXs.

NGC 1313 is a nearby face-on, late-type Sb galaxy at a distance of 3.7 Mpc (Tully 1988). The low Galactic line-of-sight absorption towards NGC 1313 ($N_{\rm H} = 0.35 \times 10^{21}$ cm^{-2}) allows us to study low energy spectral properties of sources in it. According to previous X-ray observations of NGC 1313 using the Einstein Observatory and ROSAT (Fabbiano, Trinchieri 1987; Colbert et al. 1995), its X-ray emission is dominated by three extremely luminous pointlike sources of $L_{\rm X} \sim 10^{39}$ erg s^{-1} each. One of them is the unusually luminous X-ray supernova, namely SN 1978K. The other two are typical ULXs, which we call X-1 and X-2 after Colbert et al. (1995); the former is located close ($\sim 45''$) to the galaxy nucleus.

The two ULXs have already been studied extensively with ASCA and XMM-Newton (Makishima et al. 2000; Mizuno et al. 2001; Miller et al. 2003; Dewangan et al. 2005). Observations using ASCA were used to find moderate amplitude long-term variability of these ULXs. While the spectral behavior of X-1 was rather complex, the spectrum of X-2 was represented by a hot (1.0–1.5 keV) MCD model (Mizuno 2000; Mizuno et al. 2001). The XMM spectra of both ULXs in 2000 can be represented by a power-law with soft excess, which Miller et al. (2003) interpreted as MCD emission from a cool accretion disk around a very massive ($\sim 1000\ M_{\odot}$) BH. Optical observations of X-2 indicate that the source is a high-mass X-ray binary system (Zampieri et al. 2004; Mucciarelli et al. 2005).

We conducted a Suzaku observation of NGC 1313 on 2005 October 15, with the XRT optical axis aimed at the middle point between X-1 and X-2. The data were screened based on the following standard criteria: a) The time elapsed after a passage through the South Atlantic Anomaly is longer than 256 seconds, b) The object is at least 5° and 20° above the rim of the Earth during night and day, respectively, and c) The geomagnetic cutoff rigidity is greater than 6 GeV/c. After these data screenings, the net exposure with the XIS became 27.8 ks.

The resulting XIS image of the galaxy is shown in Figure 1. The spectrum of the HXD, after subtracting the instrumental background model provided by the instrument teams, is consistent with that of the cosmic X-ray background (Boldt 1987), and no significant hard X-ray emission above 10 keV was detected.

3. Data Analysis

3.1. Light Curves of two ULXs

The 0.5–10 keV light curves of NGC1313 X-1 and X-2, extracted from the circular regions of $3'$ radius, are shown in Figure 2. The two ULXs showed clear time variability by $\sim$50%, with a flux increase for X-1 and a decrease for X-2. To investigate the change of spectral shape in a model independent way, we subtracted background extracted from a source free region of the same observation, and calculated the ratio of the spectrum of the fainter phase to that of the brighter phase. The observed ratios, shown in Figure 3, reveal intensity-correlated spectral changes in both ULXs. In X-1, the ratio stays at ~ 1 below 1 keV, and decreases toward higher energies, reaching ~ 0.6 at 3 keV and then flattening. The X-2 spectrum softens, particularly at above 3 keV, as the source gets dimmer.

In the following sections, we first analyze the time-averaged spectra to grasp rough spectral information (§ 3.2), and then study the spectral variability in detail (§ 3.3).

3.2. Time-averaged Spectra

We first calculated spectral ratios of the two ULXs to the Crab Nebula (Crab ratio). The Crab Nebula is known to have a stable, simple power-law X-ray spectrum of the photon index $\Gamma \sim 2.1$ (Toor, Seward 1974), and can be used to roughly examine the spectral property without using detector response. As shown in Figure 4, the X-1 spectrum has a flat power-law like shape below 3 keV and then falls off above 5 keV. The X-2 spectrum shows a similar shape, and is more convexed than that of X-1. Thus, neither spectrum can be expressed by a single power-law.

We then fitted the time-averaged spectra using the response matrix files as of 2006 February 13, and auxiliary response files generated by the program xissimarfgen as of 2006 April 24. Since the two ULXs exhibited the clear spectral change during the observation, here we aim at roughly evaluating spectral properties rather than quantifying the spectral parameters. We have employed the MCD plus power-law model (hereafter called "MCD+PL" model), a standard model widely used to describe the spectra of BHBs and ULXs. The data from the three FI cameras were summed together to improve the statistics. Contamination on the XIS by outgassing from the satellite (Koyama et al. 2006) and the consequent decrease in the low-energy efficiency were taken into account using the xispcoab model [1] developed by the XIS team, which

[1] http://heasarc.gsfc.nasa.gov/docs/xanadu/xspec/models/xisabs.html

empirically models the positional dependence and time evolution of the contaminant thickness of each XIS sensor based on calibration observations. Two free parameters of the model, namely the date of observation and the target offset angle from the XIS nominal position, were fixed at 63 and 3.′5, respectively; the model gave a column density of 1.0–2.9$\times10^{18}$ cm^{-2} and 0.18–0.48$\times10^{18}$ cm^{-2} for Carbon and Oxygen in the contaminant, respectively. The line-of-sight absorption outside the satellite was taken into account using the "wabs" model (Morrison, McCammon 1983), with hydrogen column density as a free parameter. Although the model approximately reproduces the data, the fit is rather poor with $\chi^2/\nu = 442.6/282$, mainly because of residuals in the 0.4–0.6 keV band and around 2 keV, as shown by Figure 5. Since the shape of the residuals around 2 keV is different between the FI and BI spectra, this is likely to be instrumental due to calibration uncertainties. We therefore excluded data in 1.5–2.3 keV in the following analysis of the X-1 spectrum. The low-energy residuals are prominent below the neutral O-edge absorption, and is suggestive of an incorrect amount of Oxygen in the spectral model. We therefore excluded, for the moment, the X-1 data below 0.6 keV, and investigate this issue in § 3.5. Neglecting the data in these two energy regions gives a marginally acceptable fit to the X-1 spectrum with $\chi^2/\nu = 256.9/218$. The X-2 spectrum, in contrast, is reproduced successfully by the MCD+PL model with $\chi^2/\nu = 152.2/142$, probably because of the limited photon statistics. We thus utilize the full energy band of the Suzaku XRT+XIS in the following spectral analysis.

The best fit model parameters describing the time averaged X-1 and X-2 spectra are tabulated in Table 1. The power-law component and the MCD component contribute almost equally to the X-1 spectrum, whereas the MCD component dominates the X-2 spectrum. These properties agree with the inference from the Crab ratio analysis. Assuming the source distance of 3.7 Mpc (Tully 1988) and isotropic radiation, the 0.4–10 keV source luminosity is obtained as 2.5×10^{40} erg s^{-1} and 5.8×10^{39} erg s^{-1} for X-1 and X-2, respectively, after correction for the absorption inside and outside the spacecraft. Even allowing for possible calibration uncertainties by $\sim10\%$, the flux of X-1 is the highest among those ever reported for this source including all archival XMM data available as of June 2006 as we confirmed through our own analysis; more than a factor of 4 higher than that of the XMM 2000 observation. The flux of X-2 is between those of the 1993 and 1995 ASCA observation, and a factor of 3 higher than that measured in the XMM observation in 2000 (Mizuno et al. 2001; Miller et al. 2003).

3.3. Spectral Variability of Each Source

To quantify the spectral change (Figure 3) associated with the intensity variations, we then divided the data into two time regions shown in Figure 2, and derived "brighter phase" and "fainter phase" spectra from the two sources. We then fitted them with several models widely used to represent the spectra of ULXs: the MCD+PL model, so called p-free disk model, and the MCD plus cutoff power-law model (hereafter MCD+cutoff-PL). The MCD+PL model is

the most commonly used description of BHB spectra, mainly those in soft state. The p-free disk model is a modified MCD model, where the disk temperature profile as a function of radius r is given as $T(r) = T_{\rm in}(r/r_{\rm in})^{-p}$ with p being a positive free parameter. This model was originally developed by Mineshige et al. (1994) to validate the standard accretion disk prediction on the temperature profile ($p = 0.75$). The model was later utilized to represent the spectra of BHBs and ULXs when the objects are thought to be in the slim disk state (e.g., Kubota, Makishima 2004), since the spectrum emergent from a slim disk is theoretically predicted to become flatter, and be approximated by the p-free disk model with p decreasing to ~ 0.5 (Watarai et al. 2000). A power-law type hard spectrum with soft excess below 1 keV has been widely observed in ULXs including those in NGC 1313 (Miller et al. 2003). Since the apparently power-law like continuum often exhibits, in close inspection, high-energy turn over (e.g., Dewangan et al. 2005; Winter, Mushotzky, Reynolds 2005), we also employed the MCD + cutoff-PL model in which the MCD component represents the excess in the soft band and the cutoff-PL represents the curved spectrum in the high energy band. The role of the MCD component in this model is different from that of the first one (MCD+PL), in which the MCD component has a high temperature and represent the high-energy spectral curvature.

All these three models are moderately successful on both the fainter-phase and brighter-phase spectra of X-1, yielding the best fit parameters as summarized in Table 2. The MCD and p-free disk models allow us to evaluate the innermost disk radius $R_{\rm in}$. After Makishima et al. (2000), we calculated this parameter as $R_{\rm in} = \xi\kappa^2\sqrt{N/\cos i}\ (D/10\ {\rm kpc})$, where N is the model normalization, i is the disk inclination angle, and D is the distance to the source; $\xi = 0.41$ and $\kappa = 1.7$ are correction factors described in Kubota et al. (1998) and Shimura, Takahara (1995). We obtained similar results on the brighter-phase X-2 spectrum: the three model are all moderately successfull, with a rather small difference in their fit goodness (Table 2). The fainter-phase spectra were reproduced by a single MCD model, and adding a power-law component with Γ=1.0-2.5 did not improve the fit significantly (less than 90% confidence using the F-test). In Table 2, we hence give only the single-MCD fit result for the fainter-phase X-2 spectrum.

3.4. Emission/Absorption Lines in X-1

The high statistics of the X-1 data have allowed us to search for emission/absorption line features. An expanded view of the time-averaged spectrum, shown in Figure 6, reveals possible absorption lines at ~ 7 keV and ~ 7.8 keV. Finer binning is used here and MCD+PL model fit gives $\chi^2/\nu = 355.4/299$. Addition of Gaussian absorption line with $\sigma = 35$ eV (width of the 5.9 keV line from the calibration source) at ~ 7 keV improves the fit by $\Delta\chi^2 = -7.9$, implying a positive detection at 96% significance from an F-test. The absorption line feature at ~ 7.8 keV is significant at the 99% confidence with $\Delta\chi^2 = -17.8$. Instrumental background of the XIS is known to weakly depend on the detector position, and the observed absorption

line features might be affected by the background uncertainty. Therefore we also used the background spectrum extracted from the same region as that of X-1, but using blank sky data, and repeated the same analysis. Again, the absorption lines are detected at ~ 7 keV and ~ 7.8 keV, at 97% and 99% confidence, respectively. We therefore conclude that these absorption line features are real. No significant emission line (at 90% confidence) is seen in the spectrum and only an upper limit can be obtained on neutral (6.4 keV) and He-like (6.7 keV) Fe K_α line. The obtained results are summarized in Table 3.

3.5. Residuals at Low Energy

Finally, we revisit the residuals seen at low energy in the X-1 spectrum. The prominent residuals are seen below the neutral O-edge absorption (Figure 5), where the model is significantly lower than the observed flux. Therefore a possible explanation of these residuals is the excess amount of Oxygen in the XIS contamination model, or the incorrect modeling of Oxygen abundance in the absorption outside the spacecraft.

To determine the abundance of Oxygen in the line-of-sight absorption, we followed the procedure of Cropper et al. (2004) and refitted the data with two absorption models: one is the wabs model with the line-of-sight absorption fixed at the Galactc value (Hydrogen column density $N_{\rm H} = 0.35 \times 10^{21}$ cm^{-2}), and the other is the "tbvarabs" absorption model (Wilms, Allen, McCray 2000) which allows us to change the abundance of each element. We used the MCD+cutoff-PL model to represent the continuum, for the model gives the smallest χ^2/ν among the three models to the brighter phase spectrum. We adopted the compilation of elemental abundances by Anders, Ebihara (1982) which provides with abundance ratios almost identical with those of "wabs" model. We first fitted the data with solar abundance, and then allowed the Oxygen abundance to change in the fitting. The improvement is significant at 99% confidence using the F-test ($\Delta\chi^2 = -50.3$) and the best-fit Oxygen abundance ratio is $0.51^{+0.11}_{-0.05}$. We further allowed the FI and BI data to have independent line-of-sight absorption and the Oxygen abundance, and obtained somewhat inconsistent abundance ratios as 0.31 ± 0.10 with $N_{\rm H} = (3.3 \pm 0.3) \times 10^{21}$ cm^{-2} and 0.68 ± 0.13 with $N_{\rm H} = (2.8 \pm 0.2) \times 10^{21}$ cm^{-2} for FI and BI data, respectively. Since FI sensors has larger low-energy intrinsic absorption than the BI sensor and may suffer from larger calibration uncertainties, we adopt the result by BI data. Then the amount of Oxygen in absorbing matter around X-1 is calculated to be smaller than that predicted by assuming solar abundance by 0.67×10^{18} cm^{-2}, which is by a factor of 3 larger than that of contamination on BI chip calculated from the xispcoab model (0.21×10^{18} cm^{-2}). Therefore the uncertainty of the contamination is negligible and we conclude that the Oxygen abundance in the absorption intrinsic to X-1 is subsolar. We also did the same analysis for X-2, i.e., first introduced two absorption models, the wabs model and tbvarabs model, to account for the Galactic line-of-sight absorption and that of the source, respectively. We then fitted the spectrum with the solar abundance and finally allowed the Oxygen abundance to change in the

fitting. Due to the limited photon statistics, the abundance is poorly constrained and only an upper limit is obtained as ≤ 1.01.

4. Discussion

In the 90 ks Suzaku observation of NGC 1313, we found luminosity changes by $\sim 50\%$ for both ULXs. The flux of X-1 is the highest among those ever observed, and the hints of absorption line features at 7–8 keV and subsolar Oxygen abundance in the line-of-sight absorption are revealed thanks to the source brightness and the good energy resolution and large effective area of Suzaku. Below we discuss the state of each ULX, mainly based on the observed spectral changes. We also discuss the environment of the X-1 system inferred from the absorption features at high and low energy.

4.1. Spectral State of X-1

NGC 1313 X-1 in the fainter phase exhibited a more or less flat spectrum with the contribution of the power-law component in the MCD+PL fit being more than 70%. In the brighter phase the spectrum is much more convex. The three models tried here all gave similar χ^2/ν, hence the goodness of the fit alone cannot tell which model is most appropriate.

The MCD+PL model reproduces the data well, and the inferred disk temperature ($T_{\rm in}$=1.3–1.6 keV) is similar to that seen in high temperature ULXs which are interpreted to be in the slim disk state (Mizuno et al. 2001; Watarai, Mizuno, Mineshige 2001). However, the contribution of the MCD component is only 20–50%; this is much smaller than in the case of high temperature ULXs where the MCD component dominates the X-ray spectrum. This results in a small inferred disk radius (~ 100 km), and the implied Schwarzschild black-hole mass (with $R_{\rm in}$ identified with three times Schwarzschild radius $R_{\rm s}$) more than an order of magnitude short of accounting for the observed luminosity within the Eddington limit. The p-free disk model fit also disfavors the slim disk interpretation. It yields somewhat worst χ^2/ν for both the fainter and brighter phase spectrum. In addition, derived increase in the temperature profile coefficient p and the decrease in the temperature $T_{\rm in}$ towards higher fluxes both contradict the theoretical prediction by the slim disk model, and previous observations of BHBs/ULXs which are thought to be in the slim disk state (e.g., Mizuno et al. 2001; Kubota, Makishima 2004). Therefore X-1 is unlikely to be in the slim disk state.

The key to understand the spectral state would be provided by the spectral ratio of the fainter phase to the brighter phase. As shown in Figure 3, spectrum below 1 keV stayed almost constant and only the hard component varied. This behavior is best represented by the MCD+cutoff-PL model fit results: the MCD component do not change the parameters significantly whereas the power-law component with exponential cutoff accounts for the source spectral change. The change of the cutoff energy is expected, e.g., when the Comptonizing electrons cool down as the source luminosity increases. The observed high energy cutoff at

4–5 keV and the large contribution of the PL component thus suggest that the disk emission is strongly Comptonized by an optically thick, relatively cool (a few keV) electron corona. We also note that such high energy curvature has been recently observed in many ULXs, e..g, Holmberg IX X-1 by Dewangan, Griffith, Rao (2006), Holmbelg II X-1 by Goad et al. (2006), many of the sample of 13 ULXs studied by Stobbart et al. (2006), 4 of the objects studied by Winter, Mushotzky, Reynolds (2005) and NGC 1313 X-1 itself by Dewangan et al. (2005). An excess at low energy is also seen from most of these ULXs, making this "soft excess plus power-law with high energy cutoff" common among bright ULXs.

A very plausible explanation of this cool component was obtained through the study of the Galactic BHB XTE J1550–564 in a very high state (Kubota, Done 2004; Done, Kubota 2005). In this state, a large fraction of the gravitational energy is dissipated from corona, in contradiction to disk dominant high/soft state. Consequently, the accretion disk is truncated to some outer radius if there exist energetically independent disk and corona (Kubota, Done 2004), or it is energetically coupled to the surrounding corona resulting in reducing the disk temperature (Done, Kubota 2005). Therefore, the XMM data (Miller et al. 2003; Dewangan et al. 2005) and Suzaku data of X-1 can be understood by inferring that the source was in a very high state, and the flux variability by more than a factor of 4 is accounted for by a varying mass accretion rate. Absorption line features at ~ 7 keV and ~ 7.8 keV support this interpretation. A marginally (at 96% confidence level) detected low energy absorption is centered at 7.04 ± 0.06 keV and is consistent with Kα absorption by H-like Fe. A significant (at 99% confidence level) absorption line at 7.81 ± 0.04 keV is thought to arise from Kα absorption from He-like Ni. Such absorption line features with equivalent widths of 20–100 eV are widely seen in Galactic BHBs when the mass accretion rate is high such as in a high/soft state or a very high state (e.g., Ueda et al. 1998; Kotani et al. 2000). Therefore, the Suzaku spectrum of X-1 supports the supposition that the system was in a very high state.

Although the error is quite large, the value of $R_{\rm in}$ we obtained is 3-4 times smaller than that measured by Miller et al. (2003) from the same source using XMM data in 2000. Dewangan et al. (2005) analyzed three XMM observations of X-1 and reported lack of the luminosity-correlated temperature changes in the soft component which would take place if the emission is emerging from a standard accretion disk. Therefore the cool disk, even if it present, is likely not extend down to $3R_{\rm s}$ but to be truncated to some outer radius, probably due to the strong Comptonization. In this case, a relatively robust estimate on the BH mass is obtained from the source luminosity. The bolometric luminosity inferred from the MCD+cutoff-PL fit to the Suzaku high flux phase data is 3.3×10^{40} erg s^{-1}, requiring a BH mass of $\sim 200\ M_{\odot}$ to satisfy the Eddington limit. Even if we allow a super-Eddington a factor of 3, a mass of 70 $M_{\odot}$ is necessary, which has never been observed in Galactic or Magellanic BHBs.

4.2. Spectral State of X-2

The fainter phase spectrum of X-2 is successfully reproduced by the MCD model alone, and the brighter phase spectrum has a flatter shape as shown by Figure 3. This spectral change coincides with the theoretical prediction by the slim disk model. P-free disk model fit gives the temperature coefficient p of the brighter phase spectrum significantly smaller than that of the standard disk ($p = 0.75$), and thus supports this interpretation. Although the observed change of the innermost disk temperature (1.85 keV to 1.25 keV) and the disk radius (46 km to 94 km) are too large to result in a flux change of 50% in this model, this could be due to the artifact by using the same spectral hardening factor κ between the fainter phase and the brighter phase; in a slim disk κ is expected to be larger than that in the standard disk (e.g., Kawaguchi 2003; Watarai, Mineshige 2003). Another possible explanation of the observed softening of the spectrum and the flux decrease is a disappearance of a weak power-law component, as inferred by the MCD+PL fit result. Such a power-law component is sometimes seen in galactic BHBs thought to be in the slim disk state (Kubota, Makishima 2004). Although the error is large, the resultant change of $T_{\rm in}$ and $R_{\rm in}$ follows the $T_{\rm in} \propto R_{\rm in}^{-1}$ relation as predicted by the slim disk model (Watarai et al. 2000). Either model thus suggests that the spectral change can be understood by the slim disk scenario, and confirms the previous ASCA result that the source is in a slim disk state when the luminosity is high. The X-2 can be understood as a $\sim 50\ M_\odot$ BHB shining close to the Eddington limit whose innermost disk radius is a factor of 5 smaller than that inferred from the BH mass, due to the BH spinning and/or the characteristics of the slim disk (e.g., Makishima et al. 2000; Mizuno et al. 2001). We also note that from XMM data in 2000 observation (Miller et al. 2003) the source was a factor of 3 less luminous than the Suzaku fainter phase data. The XMM data were reproduced by a power-law model with $\Gamma = 1.8$ and with soft excess emission, and could be understood by inferring that the source was in a very high state.

4.3. Absorption line features of X-1

Two possible absorption line features have been found in the X-1 spectrum, one marginally (at 96% confidence) at ~ 7 keV but the other more significantly at 99% confidence at ~ 7.8 keV. Such line features are commonly seen in Galactic BHBs (e.g., Ueda et al. 1998; Kotani et al. 2000), and confirm the presence of a highly ionized plasma along the line of sight from the continuum source, probably above the accretion disk. The central energy of the lower-energy absorption line, 7.04 ± 0.06 keV, is roughly consistent with that of the He-like Fe Kα absorption line (6.95–6.97 keV). The high-energy one at ~ 7.8 keV could be a blend of He-like Ni Kα (7.77-7.81 keV) and He-like Fe Kβ (7.88 keV). Since the 6.7 keV He-like Fe Kα absorption line is not seen in the data (the 90% confidence upper limit on the equivalent width is 10 eV), the contribution of He-like Fe Kβ to the high energy absorption line is considered negligible. Thus, this high energy feature may be identified with the Kα absorption of He-like

Ni. Such a strong line at ~ 7.8 keV is sometimes seen in Galactic BHBs (e.g., Kotani et al. 2000; Sala et al. 2006).

From the observed equivalent widths of the absorption lines, we can estimate the column density of the line-absorbing plasma, using a "curve of growth" computed by Kotani et al. (2000). The result depends on the assumed line-of-sight velocity dispersion of the ions, $(2kT_{\rm kin}/m)^{1/2}$, where k is the Boltzman constant, $T_{\rm kin}$ is the "kinetic" temperature of the ions including both the thermal motion and the bulk motion, m is the mass of an iron or nickel atom: a larger velocity dispersion enables a lower column density to produce the same equivalent width. The plasma needs to be optically thin to Thomson scattering (e.g., $N_{\rm H} \leq 1.5 \times 10^{24}$ cm^{-2}), so that the resonance lines should be observed. This requires $\log N_{\rm Fe} \leq 19.7$ and $\log N_{\rm Ni} \leq 18.4$ if we take the solar abundance of Morrison, McCammon (1983). Unfortunately, the large errors associated with the Fe absorption line feature do not allow us to constrain the plasma parameters. On the other hand, the observed equivalent width of He-like Ni Kα, 79^{+43}_{-38} eV, corresponds to $\log N_{\rm Ni} = 19.8^{+0.5}_{-1.1}$ and $18.7^{+1.2}_{-0.8}$ for $kT_{\rm kin} = 10$ keV and 100 keV, respectively. Therefore the kinematic temperature of the plasma should be higher than a few tens of keV to account for the observed equivalent width unless nickel is highly overabundant. Such a high temperature is unlikely to be thermal, because then most of the nickel atoms would be then fully ionized. Since the thermal motion then becomes negligible, the line-of-sight velocity dispersion of a few hundred km s^{-1}, corresponding to a $kT_{\rm kin}$ = of a few tens of keV, is mostly attributed to bulk motions. Similar high kinematic temperatures have been found from BHBs such as GRS 1915+105 (Kotani et al. 2000) and GRO J1655–40 (Yamaota et al. 2001), and interpreted as arising from plasma bulk motions. For the Galactic low-mass X-ray binary GX13+1, a velocity dispersion of ~ 500 km s^{-1} and a blue shift of ~ 400 km s^{-1} were measured and thought to be due to a disk wind (Ueda et al. 2004). It is thus likely that mass outflow of a few hundred km s^{-1} accounts for the line-absorbing plasma, although the limited photon statistics prevent us from reaching any firm conclusion.

4.4. Oxygen Abundance

The best fit Oxygen abundance in the absorption intrinsic to X-1 is significantly lower than the solar value and is measured to be 0.68 ± 0.13 relative to that given by Anders, Ebihara (1982), resulting in an Oxygen to Hydrogen number ratio of $\mathrm{O/H} = (5.0 \pm 1.0) \times 10^{-4}$. This value is consistent with that of the interstellar medium (ISM) in compilation by Wilms, Allen, McCray (2000). It is thus likely that the Oxygen abundance in the ISM is subsolar in NGC 1313 as well as in the Milkey Way. We also note that recent measurements of solar Oxygen abundance are reconciled with the ISM Oxygen abundance, as discussed by Baumgartner, W. H., Mushotzky, R. F. (2006).

5. Summary

We have analyzed Suzaku data from NGC 1313 which hosts two famous ULXs, X-1 and X-2, and found that both showed luminosity change by about 50% in the 90 ks observation. X-1 showed the highest X-ray flux among those ever observed and the spectrum exhibited a strong power-law component with a high energy cutoff at 4–5 keV which accounts for the spectral change. Thanks to the high flux of the source, the high throughput of the Suzaku XRT and the good energy resolution of the Suzaku XIS in the Fe line energy range, hints of absorption line features are found at ~ 7.0 keV and ~ 7.8 keV with equivalent widths of 40–80 eV for the first time. These spectral properties support the hypothesis that the source was in a very high state. The high sensitivity in the low energy range and the small amount of contamination during this period of observation have enabled us to measure the Oxygen abundance of the X-1 system to be subsolar but consistent with the recent value of ISM. The X-2 spectrum in the fainter phase is well represented by a MCD model of $T_{\rm in} = 1.2$–1.3 keV and becomes flatter as the source gets more luminous, confirming the previous result that the source is in a slim disk state when the luminosity is high. BHs of mass of $\sim 200\ M_\odot$ and $\sim 50\ M_\odot$ are required for X-1 and X-2, respectively, to explain the observed luminosity within the Eddington limit.

We would like to thank N. White and Suzaku managers for helpful discussions. We also thank all the Suzaku team members for their dedicated support of the satellite operation and calibration.

Table 1. Time-averaged ULX spectra fitted with the MCD+PL model

source	$N_{\rm H}$* (10^{21} cm^{-2})	$T_{\rm in}$ (keV)	$f_{\rm disk}$†	Γ	$f_{\rm pow}$‡	χ^2/ν
X-1§	2.1 ± 0.3	1.60 ± 0.15	7.03	$2.08^{+0.17}_{-0.21}$	8.57	256.9/218
X-2	$1.1^{+0.7}_{-0.2}$	1.29 ± 0.08	2.68	$1.17\leq1.89$	0.88	152.2/142

Notes. Errors are calculated for 90% confidence for one interesting parameter ($\Delta\chi^2=2.7$)

* Hydrogen column density of the photoelectric absorption

† 0.4–10 keV flux of the MCD component in units of 10^{-12} erg s^{-1} cm^{-2} after removing the absorption

‡ 0.4–10 keV flux of the PL component in units of 10^{-12} erg s^{-1} cm^{-2} after removing the absorption

§ Data below 0.6 keV and in the region 1.5–2.3 keV are not used for the spectral fitting.

Table 2. Fits to time-sorted spectra with errors for 90% confidence for one interesting parameter

model	$N_{\rm H}$ (10^{21} cm^{-2})	$T_{\rm in}$ (keV)	$R_{\rm in}$ ($\frac{1}{\cos i}$km)	Γ or p	$E_{\rm c}$ (keV)	$f_{\rm disk}$*	$f_{\rm pow.}$†	χ^2/ν
			X-1‡					
fainter phase								
MCD+PL	2.4 ± 0.7	$1.30^{+0.65}_{-0.36}$	89^{+106}_{-44}	$2.09^{+0.41}_{-0.26}$		2.32	10.37	82.5/94
p-free	2.3 ± 0.2	$2.69^{+0.88}_{-0.38}$	$21(\leq31)$	0.514 ± 0.014		12.47		83.9/95
MCD+cutoff-PL	$3.0^{+2.1}_{-1.5}$	$0.20(\leq0.41)$	$4500(\leq25000)$	$1.59^{+0.33}_{-0.60}$	$6.04^{+6.84}_{-2.27}$	1.92	11.72	82.1/93
brighter phase								
MCD+PL	2.0 ± 0.4	$1.63^{+0.13}_{-0.17}$	107^{+23}_{-11}	2.03 ± 0.24		8.31	8.00	240.4/218
p-free	1.8 ± 0.2	2.09 ± 0.10	60 ± 7	0.595 ± 0.012		15.58		243.4/219
MCD+cutoff-PL	$2.3^{+0.5}_{-0.8}$	$0.21^{+0.13}_{-0.03}$	3800^{+6700}_{-3200}	0.89 ± 0.20	$3.41^{+0.57}_{-0.40}$	1.48	15.13	237.9/217
			X-2					
fainter phase								
MCD	0.9 ± 0.3	1.24 ± 0.05	96 ± 9			2.28		71.2/76
brighter phase								
MCD+PL	$1.6^{+0.7}_{-0.4}$	$1.39^{+0.24}_{-0.14}$	80^{+30}_{-20}	$1.62^{+0.58}_{-1.09}$		2.59	1.61	148.9/142
p-free	1.7 ± 0.4	1.86 ± 0.15	43^{+12}_{-9}	$0.627^{+0.36}_{-0.26}$		4.20		150.8/143
MCD+cutoff-PL	2.1 ± 0.9	$0.24(\leq0.57)$	$1300(\leq4600)$	$0.59^{+0.27}_{-0.41}$	$2.61^{+0.58}_{-0.47}$	0.36	4.01	147.6/141

* 0.4–10 keV flux of the MCD or the p-free disk component in unit of 10^{-12} erg s^{-1} cm^{-2} after removing the absorption

† 0.4–10 keV flux of the cutoff PL component in unit of 10^{-12} erg s^{-1} cm^{-2} after removing the absorption

‡ Data below 0.6 keV and within the range 1.5–2.3 keV are not used for the spectral fitting.

Table 3. Parameters for emission/absorption line features in the spectrum of NG1313 X-1. Errors are for 90% confidence or 90% upper limit.

component	Energy (keV)	EW (eV)	significance
absorption 1	7.04 ± 0.06	45^{+30}_{-33}	96%
absorption 2	7.81 ± 0.04	79^{+43}_{-38}	99%
line 1	6.40 (fixed)	≤ 62	
line 2	6.70 (fixed)	≤ 87	

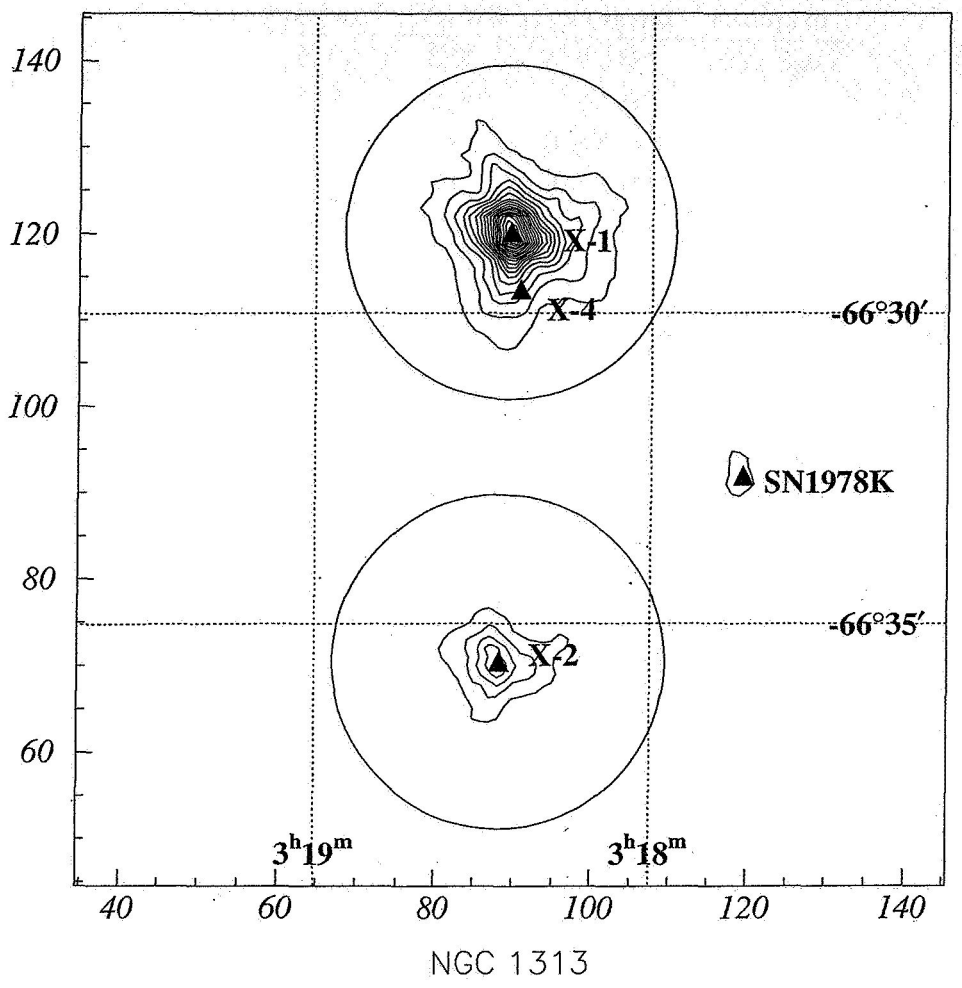

Fig. 1. An XIS 0 image of the NGC 1313 region in the 0.4–10 keV band, where we can see X-1, X-2 and SN 1978K as local peaks in the X-ray contours. The image was smoothed using a gaussian distribution with $\sigma = 0.'1$. Triangles indicate the positions of strong X-ray sources detected in the ROSAT HRI observation (Schlegel et al. 2000), shifted by $0.'65$ which is within the pointing accuracy of the Suzaku satellite. Also shown are the accumulation regions for source spectra. Note that source names are after Colbert et al. (1995).

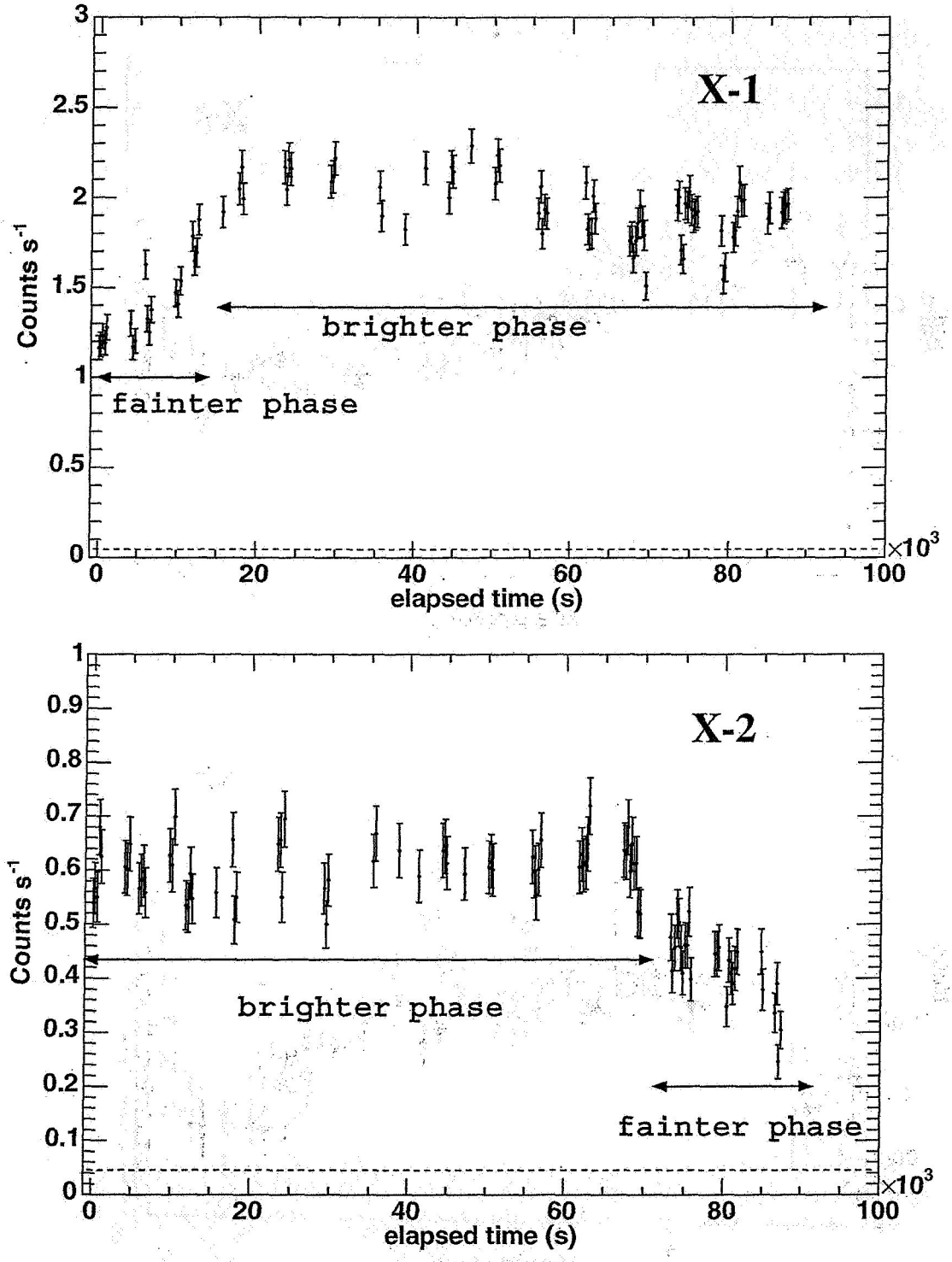

Fig. 2. Suzaku FI light curves for X-1 (top panel) and X-2 (bottom panel) in the 0.4–10 keV energy range with 256 s binning. Background is included and the background level is indicated by dotted lines. Also shown are the time intervals used to study the short-term spectral variability.

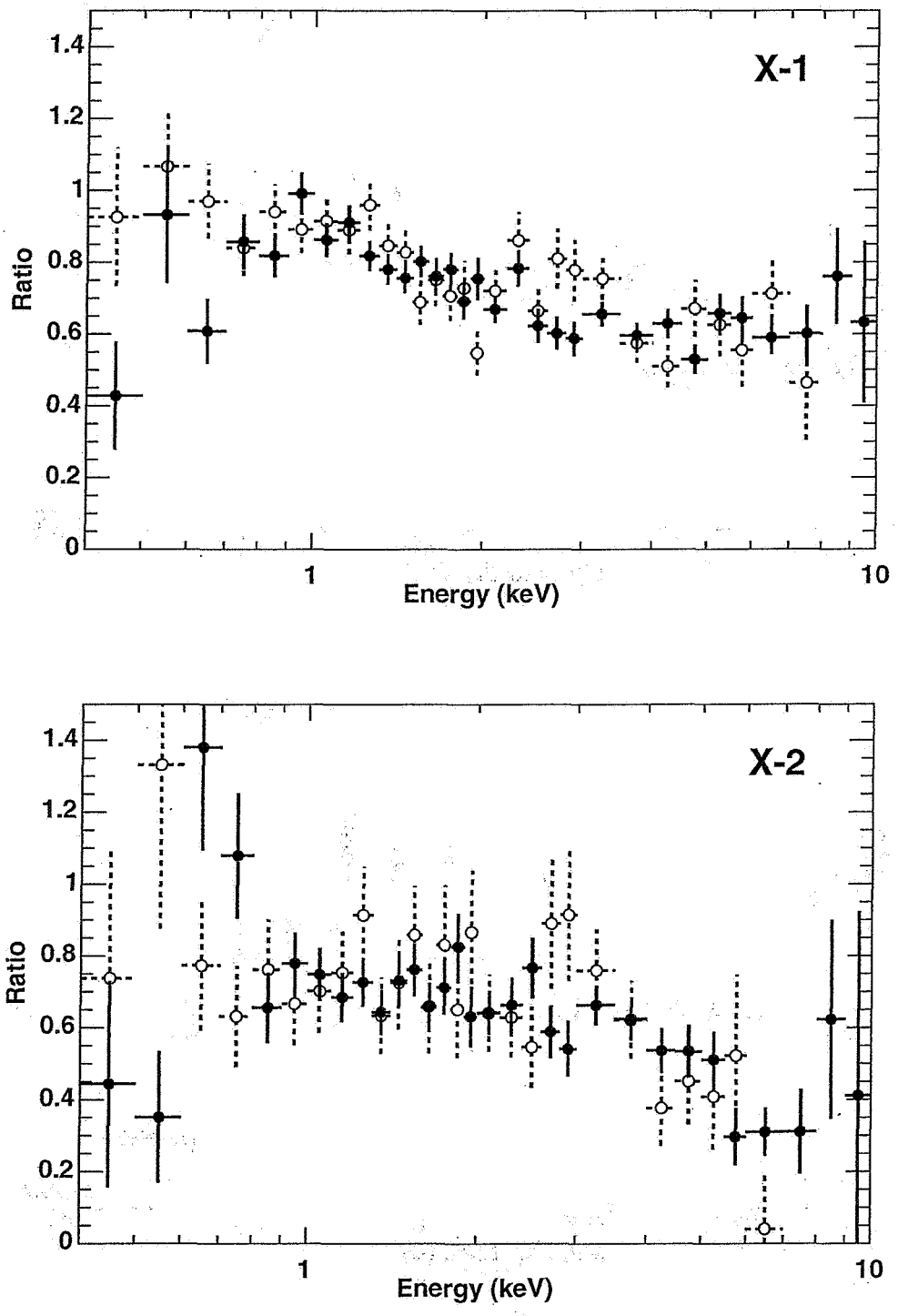

Fig. 3. Spectral ratio of the fainter phase to the brighter phase for X-1 (top panel) and X-2 (bottom panel), after subtracting the background. The ratio of FI and BI data are given as filled circles and open circles, respectively.

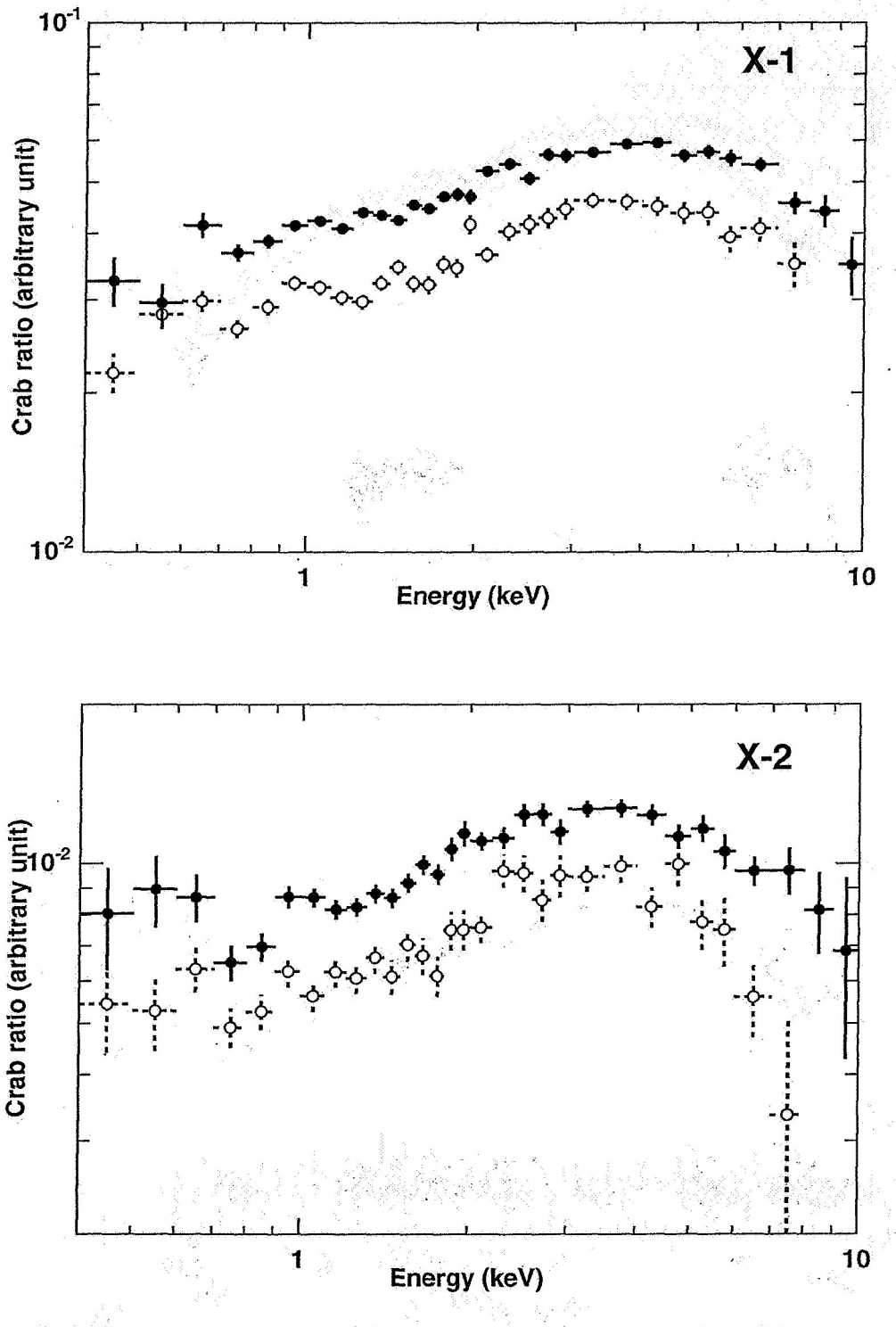

Fig. 4. Crab ratio of the time-averaged spectra for X-1 (top panel) and X-2 (bottom panel), after subtracting the background for two ULXs. Symbols are the same as those of Figure 3. FI data are shifted up for clarity.

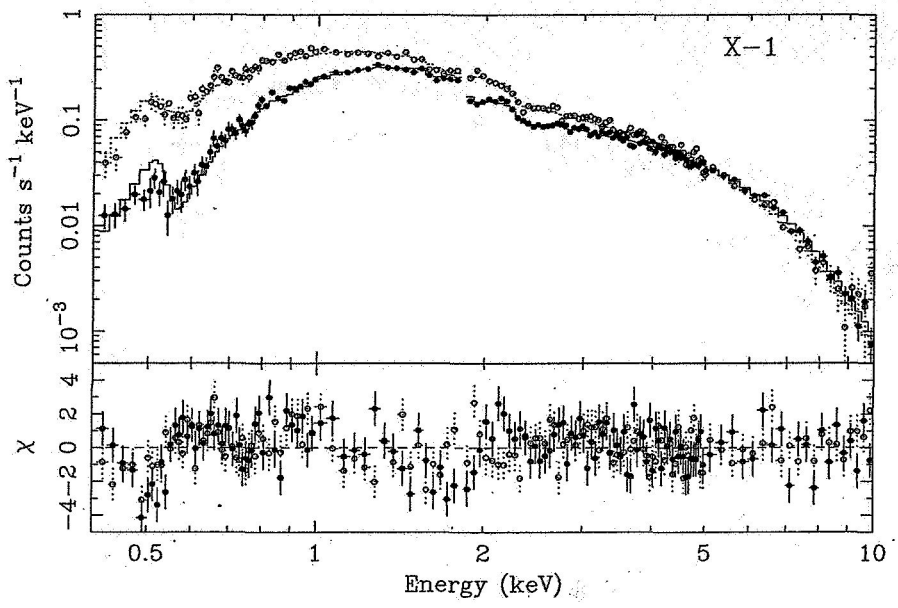

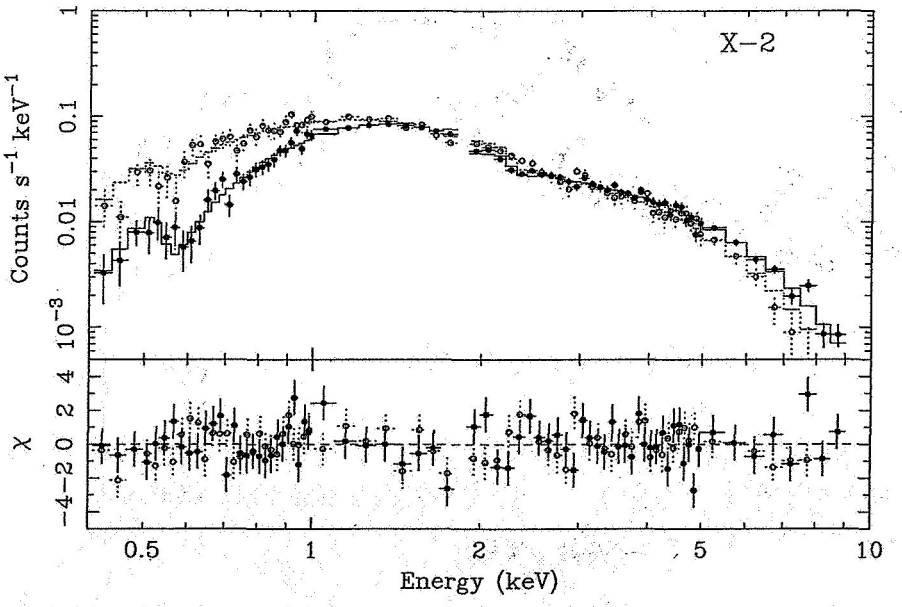

Fig. 5. Time averaged XIS spectra of NGC 1313 X-1 (top panel) and X-2 (bottom panel) fitted with the MCD+PL model. The histogram shows the best fit model and crosses represent the observed spectra. The bottom panel shows the fit residuals. The FI and BI spectra, shown with solid-line and dotted-line crosses, respectively, are fitted simultaneously except for the relative normalization. Since the gain gap due to the Si K edge is not properly handled in the current pipeline processing, data of PI channel 500–504 are ignored.

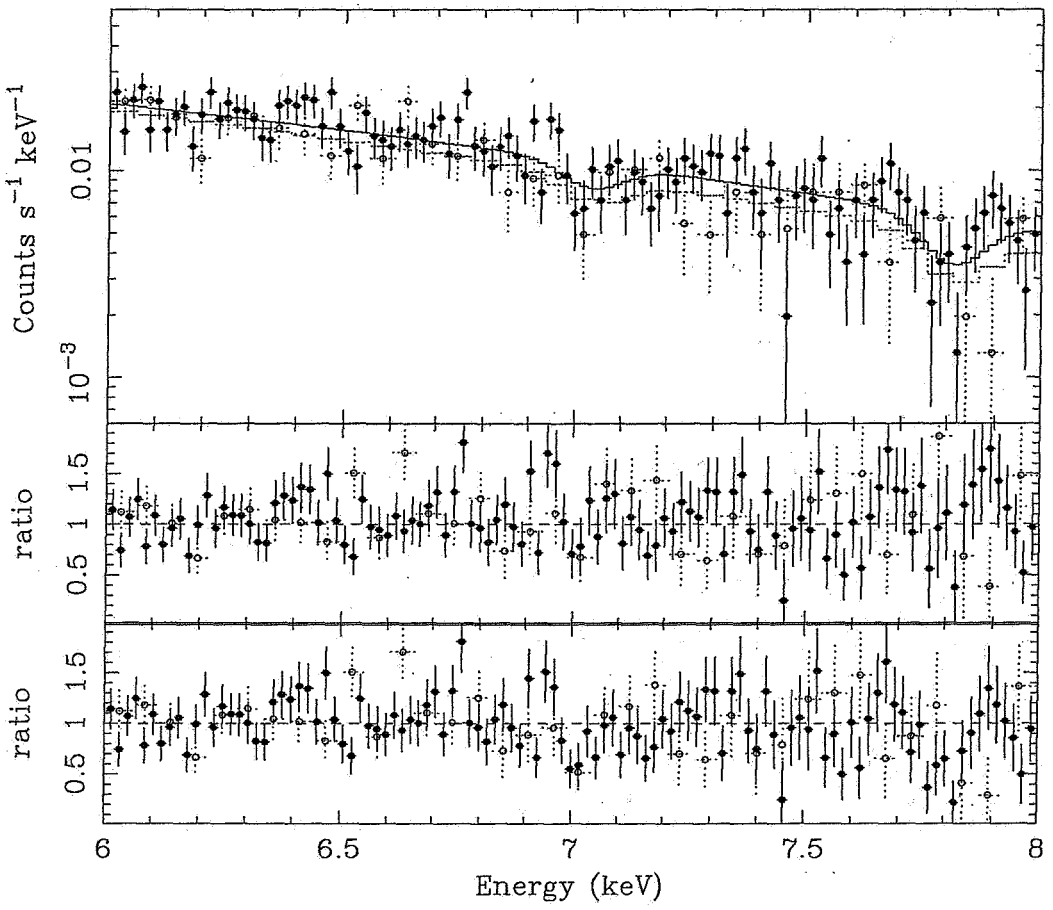

Fig. 6. Expanded view of the 6–8 keV spectrum of X-1. The top and middle panels show the data with best fit model and the fit residuals, respectively. Absorption lines at $\sim$7 keV and $\sim$8 keV are added to the continuum represented by the *MCD+PL* model. The bottom panel shows the residuals when we remove these absorption lines. Symbols are the same as those of Figure 4.

References

Abramowicz, M. A., Czenry, B., Lasota, J. P., & Szuszkiewicz, E. 1988, ApJ, 332, 646

Anders, E., & Ebihara, M. 1982, Geochimica et Cosmochimica Acta, 46, 2363-2380

Baumgartner, W. H. & Mushotzky, R. F. 2006, ApJ, 639, 929

Boldt, E. 1987, IAU Circ., 124, 611

Colbert, E. J. M., Petre, R., Schlegel, E. M. & Ryder, S. D. 1995, ApJ, 446, 177

Colbert, E. J. M. & Mushotzky, R. F. 1999, ApJ, 519, 89

Cropper, M., Soria, R., Mushotzky, R. F., Wu, K., Markwardt, C. B. & Pakull, M. 2004, MNRAS, 349, 39

Dewangan, G. C., Griffiths, R. E. & Rao, A. R. 2005, astro-ph/0511112

Dewangan, G. C., Griffiths, R. E. & Rao, A. R. 2006, ApJ, 641, 125

Done, K. & Kubota, A. 2005, astro-ph/0511030, accepted in MNRAS

Ebisawa, K., Zychi, P, Kubota, A., Mizuno T. & Watarai, K. 2003, ApJ, 597, 780

Fabbiano, G. 1989, ARA&A, 27, 87

Fabbiano, G. & Trinchieri, G. 1987, ApJ, 315, 46

Feng, H. & Kaaret, P. 2005, ApJ, 633, 1052

Foschini, L., et al. 2002, A&A, 392, 817

Goad, M. R., Robert, T. P., Reeves, J. N. & Utteley, P. 2006, MNRAS365, 191

Kawaguchi, T. 2003, ApJ, 593, 69

Kobayashi, Y., Kubota, A., Nakazawa, K., Takahashi, T. & Makishima, K. 2003 PASJ, 55, 273

Kokubun, M., et al. 2006, PASJ, this volume

Kotani, T., Ebisawa, K., Dotani, T., Inoue, H., Nagase, F., Tanaka, Y. & Ueda, Y. 2000, ApJ, 539, 413

Erratum: ApJin preass, astro-ph/0003237

Koyama, K., et al. 2006, PASJ, this volume

Kubota, A., Tanaka, Y., Makishima, K., Ueda, Y., Dotani, T., Inoue, H. & Yamaoka, K., PASJ, 50, 667

Kubota, A., Mizuno, T., Makishima, K., Fukazawa, Y., Kotoku, J., Ohnishi, T., and Tashiro, M. 2001a, ApJ, 547, L119

Kubota, A., Makishima, K. & Ebisawa, K. 2001b ApJ, 560, L147

Kubota, A., Done, C. & Makishima, K. 2002, MNRAS, 337, L11

Kubota, A. & Makishima, K. 2004, ApJ, 601, 428

Kubota, A., & Done, C., 2004 MNRAS, 353, 980

Makishima, K., et al. 2000, ApJ, 535, 632

McClintock, J. E. & Remillard, R.A. 2003, in Compact Stellar X-ray Sources, ed. Lewin, W. H. G. & van der Klis, M. (Cambridge: Cambridge Univ. Press), 157

Miller, J. M., Fabbiano, G., Miller, M. C. & Fabian, A. C. 2003, ApJ, 585, L37

Miller, J. M., Fabian, A. C. & Miller, M. C. 2004, ApJ, 607, 931

Mineshige, S, Hirano, A., Kitamoto, S., Yamada, T., Fukue, J. 1994, ApJ, 426, 308

Mitsuda, K., et al. 1984, PASJ, 36, 741

Mitsuda, K., et al. 2006, PASJ, this volume

Mizuno, T. 2000, Ph.D thethis, Univ. Tokyo
Mizuno, T., Kubota, A. & Makishima, T. 2001, ApJ, 554, 1282
Miyamoto, S., Kimura, K., Kitamoto, S., Dotani, T. & Ebisawa, K. 1991, ApJ, 383, 784
Morrisson, R. & McCammon, D. 1983, ApJ, 270, 119
Mucciarelli, P., Zampieri, L., Falomo, R., Turolla, R., Treves, A. 2005, ApJ, 633, L101
La Parola, V., Peres, G., Fabbiano, G., Kim, D. W. & Bocchino, F. 2001, ApJ556, 47
Okada, K., Dotani, T., Makishima, K., Mitsuda, K., & Mihara, T., 1998, PASJ, 50, 25
Sala, G., Greiner, J., Vink, J., Haberl, F., Kendziorria, K. & Zhang, X. L. 2006, astro-ph/0606272
Schlegel, E. M., Petre, R., Colbert, E. J. M. & Miller, S. 2000, ApJ, 120, 2373
Serlemitsos, P., et al. 2006, PASJ, this volume
Shimura, T. & Takahara, F., 1995, ApJ, 445, 780
Stobbart, A.-M., Roberts, T. P. & Wilms, J. 2006, MNRAS, 368, 397
Swartz, D. A., Ghosh, K. K., Tennant, A. F. & Wu, K. 2004, ApJS, 154, 519
Szuszkiewicz, E., Malkan, M. A. & Abramowicz, M. A. 1996, ApJ, 458, 474
Takahashi, T., et al. 2006, PASJ, this volume
Toor, A. & Seward, F. D. 1974, ApJ79, 995
Tully, R. B. 1988, Nearby Galaxies Catalogue (Cambridge: Cambridge Univ. Press)
Ueda, Y., Inoue, H., Tanaka, Y., Ebisawa, K., Nagase, F., Kotani, T. & Gehrels, N. 1998, ApJ, 492, 782
Ueda, Y., Murakami, H., Yamaoka, K., Dotani, T. & Ebisawa, K. 2004, ApJ, 609, 325
Walsh, J. R. & Roy, J.-R. 1997, MNRAS, 288, 726
Watarai, K., Fukue, J., Takeuchi, M. & Mineshige, S. 2000, PASJ, 52, 133
Watarai, K., Mizuno, T. & Mineshige, S. 2001, ApJ, 549, L77
Watarai, K., & Mineshige, S. 2003, ApJ, 596, 421
Wilms, J., Allen, A. & McCray, R. 2000, ApJ542, 914
Winter, L. M., Mushotzky, R. F. & Reynolds, C. S. 2005, astro-ph/0512480, accepted for ApJ
Yamaoka, K., Ueda, Y., Inoue, H., Nagase, F., Ebisawa, K., Kotani T., Tanaka, y. & Zhang, S. N. 2001, PASJ, 53, 179
Zampieri, L., Mucciarelli, P., Falomo, R., Kaaret, P., di Stefano, R., Turolla, R., Chieregato, M. & Treves, A. 2004, Nuclear Physics B, 132, 387